Universiteit
Leiden
The Netherlands

Immunotherapy for human cancer : from bedside to bench and back

Kelderman, S.

Citation
Kelderman, S. (2016, November 30). *Immunotherapy for human cancer : from bedside to bench and back*. Retrieved from https://hdl.handle.net/1887/44515

Version:	Not Applicable (or Unknown)
License:	Licence agreement concerning inclusion of doctoral thesis in the Institutional Repository of the University of Leiden
Downloaded from:	https://hdl.handle.net/1887/44515

Note: To cite this publication please use the final published version (if applicable).

Cover Page

Universiteit Leiden

The handle http://hdl.handle.net/1887/44515 holds various files of this Leiden University dissertation.

Author: Kelderman, S.
Title: Immunotherapy for human cancer : from bedside to bench and back
Issue Date: 2016-11-30

Chapter 8

Neo-antigen enriched TIL therapy mediates superior tumor control in a xenograft model of human melanoma

Sander Kelderman[1#], Laura Bies[1#], Marit M. van Buuren[1], Nienke van Rooij[1], Daisy Philips[1], Mireille Toebes[1], Laura J.A. van Dijk[1], Samira Michels[1], Lorenzo Fanchi[1], Bianca Weißbrich[4], Kristel Kemper[1], Daniel S. Peeper[1], Sam Behjati[2], Michael R. Stratton[2], Lothar Germeroth[3], Bianca Heemskerk[1], Dirk H. Busch[4], Chantale Bernatchez[5], Laszlo G. Radvanyi[5], Christian U. Blank[1], Patrick Hwu[5], John B.A.G. Haanen[1], Pia Kvistborg[1], and Ton N.M. Schumacher[1]

[1]The Netherlands Cancer Institute NKI-AVL, Amsterdam, The Netherlands, [2]Cancer Genome Project, Wellcome Trust Sanger Institute, Hinxton, United Kingdom, [3]Stage Cell Therapeutics GmbH, Göttingen, Germany, [4]Technische Universität München, Munich, Germany, [5]MD Anderson Cancer Center, Houston, USA. [#] These authors contributed equally to this work

Manuscript submitted

INTRODUCTION

In cancers with a high mutational load, such as melanoma, lung and colorectal cancer[1,2], large numbers of mutated peptides (hereafter referred to as neo-antigens) are potentially presented by MHC class I and II molecules on the surface of tumor cells[3-5]. Furthermore, recent reports have demonstrated that neo-antigen-specific T-cell reactivity is frequently observed in melanoma[5-9]. However, the contribution of neo-antigen specific T-cell reactivity to tumor control is only partially understood. In this report, we explore the potential clinical relevance of neo-antigens that are recognized by $CD8^+$ T cells. We first demonstrate how treatment with a clinically effective TIL product can lead to the marked dominance of a neo-antigen specific T-cell response in a patient with melanoma. We then provide direct evidence in a patient-derived xenograft model of human melanoma that T-cell responses against neo-antigens can mediate superior tumor regression as compared to bulk TIL. Finally, we show that within this patient, the anti-tumor potential of neo-antigen specific T-cell receptors is greater than that of T-cell receptors directed against the Cancer/Germline antigen family. Collectively, these data provide support for the selective targeting of neo-antigens in cancer immunotherapy.

RESULTS

For this study, we obtained tumor tissue from a 46-year old female patient (MDACCTIL2379) suffering from metastatic melanoma who underwent treatment with $100x10^9$ autologous TIL according to a previously described clinical protocol[10]. Radiologic evaluation six weeks post TIL infusion showed a rapid clinical response, with a more than 50% decrease of baseline tumor burden. Seven months post-therapy, the patient was in complete remission, and continues to be so at two years of follow-up (Supplementary Fig. 1A). Based on the fact that T-cell responses against neo-antigens are not hampered by central T-cell tolerance, an important role of such T-cell reactivities in anti-tumor immune responses has previously been postulated[6,11-13]. Furthermore, through the development of cancer exome sequencing approaches and high-throughput immunomonitoring technology, it is now possible to evaluate T-cell reactivity against neo-antigens within individual patients. By this method, T-cell responses against neo-antigens have been observed in T-cell products successfully used for therapy, including one case in which infusion of a $CD4^+$ T-cell population with high reactivity towards a neo-antigen was shown to lead to a reduction in tumor burden[14]. To address the potential involvement of neo-antigen directed T-cell reactivity in the tumor response of patient MDACCTIL2379, we performed whole-exome sequencing on a primary melanoma cell line obtained from this patient to identify somatic tumor mutations (Fig. 1A).

A total of 960 non-synonymous mutations were found, (953 substitution and 7 insertions/deletions, FDR 0.07). As expected, substitutions were predominantly C>T/G>A transitions enriched at dipyrimidine sequences indicative of a UV-induced mutational signature[1] (Supplementary Fig. 1B, left). Next, mutations present within expressed genes were identified using RNAseq data, and 39 amino-acid stretches encompassing these mutations were used for the prediction of potential neo-antigens (Fig. 1A). Using a low cut-off to avoid false negatives, this resulted in 1,008 potential CD8 T-cell epitopes for HLA-A*01:01, HLA-A*23:01 and HLA-B*55:01. Subsequently, the autologous TIL culture of this patient was analyzed for the presence of neo-antigen reactive T-cell populations against any of these peptides, by combinatorial coding with a library of peptide-MHC (pMHC) complexes generated through UV-induced peptide exchange[15-17]. This screen revealed the presence of two neo-antigen reactive T-cell populations within the TIL infusion product: one low-level response (0.17% of $CD8^+$ T cells), specific for a mutation in the RASSF1 (RAS association domain family member 1) gene product, and one very dominant response (23% of $CD8^+$ T cells within the infusion product), specific for a mutation in the *DHX33* (DEAH box polypeptide 33) gene product (Fig. 1B).

To reveal whether T-cell reactivity against these neo-antigens was substantially influenced by TIL therapy, pre- and post-therapy PBMC samples were analyzed by staining with MHC multimers loaded with the $RASSF1_{R244C}$ and $DHX33_{R186W}$ neo-epitopes. Within pre-therapy PBMC, total T-cell responses against the two neo-antigens were barely detectable (0.011% of $CD8^+$ T cells). However, at day 7 post-infusion, approximately 50% of peripheral blood T cells were directed against the single neo-antigen within *DHX33*, and this T-cell response expanded further in the subsequent weeks to approximately 62%, a more than 6,800-fold increase relative to pre-therapy levels (Fig. 1C and Supplementary Fig. 1C).

Prior data have shown the common occurrence of neo-antigen specific $CD8^+$ T-cell responses in TIL products[8,9,18], and the above data demonstrate that T-cell responses against a mutated antigen can subsequently dominate the T-cell compartment at the time of clinical response. Nevertheless, this type of clinical data can only provide correlative evidence for the importance of neo-antigen reactive T cells. To evaluate the relevance of neo-antigen specific T-cell reactivity in a more direct manner, we aimed to develop a system in which the activity of different T-cell populations against autologous tumor could be analyzed in parallel. For this purpose, we studied tumor tissue and TIL obtained from a 61-year old female patient with metastatic melanoma (NKIRTIL006) who had undergone a palliative metastasectomy in 2005 and never received any form of immunotherapeutic intervention. From the tumor digest, TIL and tumor cell line cultures were established in parallel and tumor tissue was used for both whole exome sequencing and to generate a PDX model in NOD-SCID-IL2R gamma-chain deficient (NSG) mice. Within the tumor of this patient, a total of 350 non-synonymous mutations were identified (Supplementary Fig. 1B, right) and, using

our epitope prediction pipeline, 252 potential neo-antigens were predicted. Subsequent screening of autologous TIL with an MHC multimer library containing these epitopes led to the identification of three neo-antigen reactive T-cell populations within this patient: (1) a T-cell response (1.604% of $CD8^+$ T cells) directed against an R24L mutation in the *CDK4* (cyclin-dependent kinase 4) gene product; (2) a T-cell response (0.407% of $CD8^+$ T cells) directed against a mutation in the *GCN1L1* (general control of amino-acid synthesis 1-like 1) gene product; (3) a low-magnitude (0.003%) T-cell response directed against a mutation in the *DNAH17* (dynein axonemal heavy chain 17) gene product (Fig. 1D).

In order to compare the relative activity of neo-antigen specific T cells versus that of standard TIL, we developed a T-cell enrichment procedure that uses HLA-A*0201 UV-exchange streptamers to purify T-cell populations of interest and utilized this to enrich for the $GCN1L1_{L2330P}$ and $CDK4_{R24L}$ -specific HLA-A*02:01 restricted T-cell responses[19]. Both the enriched cell culture (92.4% total $GCN1L1_{L2330P}$ and $CDK4_{R24L}$ reactivity) and the standard bulk culture (2.78% total $GCN1L1_{L2330P}$ and $CDK4_{R24L}$ reactivity) were expanded according to a rapid expansion protocol (REP)[10] that is used to create TIL products for treatment (Supplementary Fig. 1D). High functional activity of the enriched T-cell product towards the two mutant epitopes was established by analysis of intracellular cytokine secretion upon coculture of T cells with HLA-A*02:01 restricted target cells loaded with either the mutant epitope or the wild type counterpart (Fig. 1E). Notably, a subsequent coculture of the standard TIL and the enriched TIL with the autologous tumor cell line revealed a more modest increase in reactivity and tumor cell killing (Fig. 1F and Supplementary Fig. 1E).

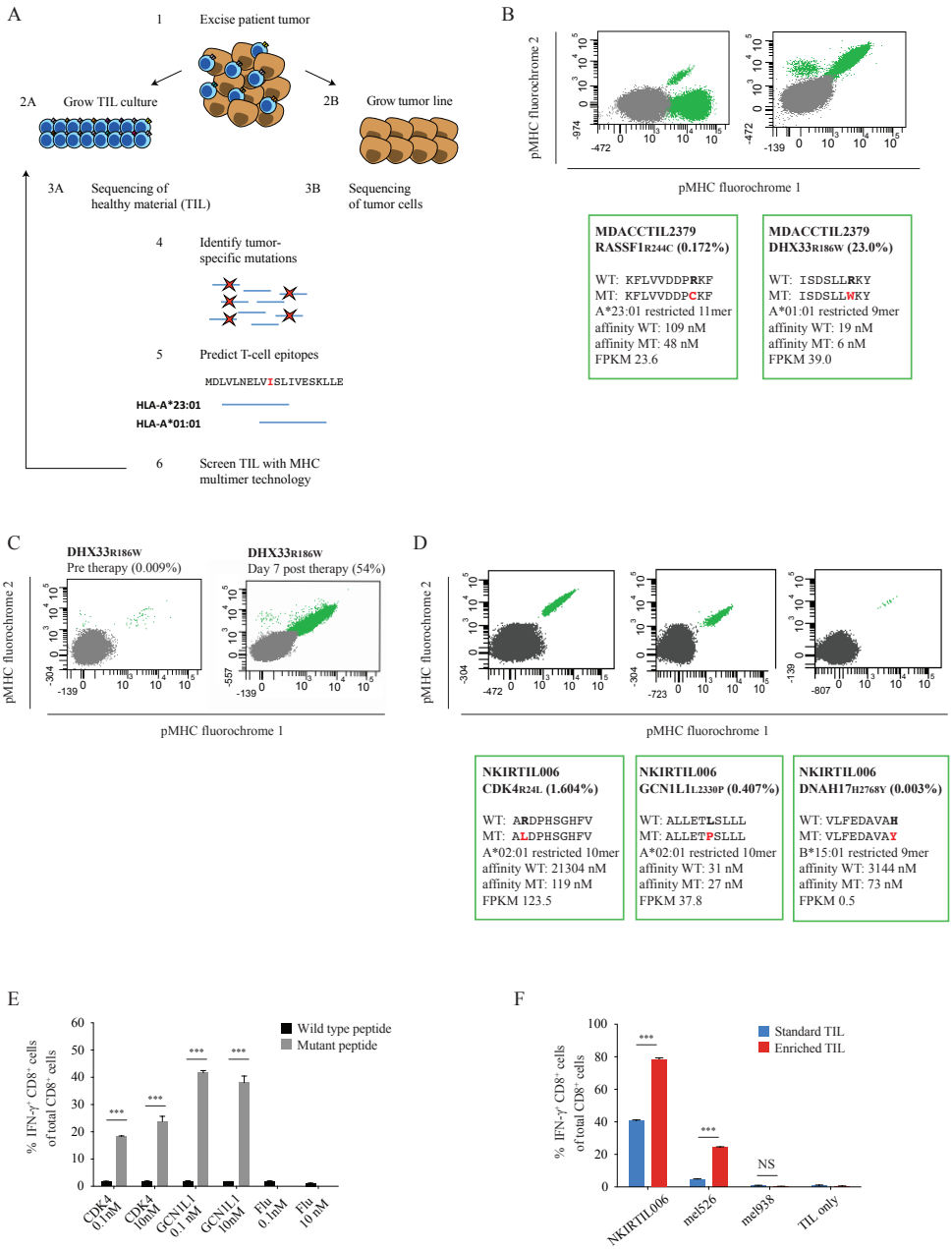

Figure 1. Neo-antigen reactive T-cell populations in human melanoma TIL cultures. (a) Overview of methods used to identify neo-antigen reactive CD8⁺ T cells in bulk melanoma tumor-infiltrating lymphocytes (TIL) cultures. Brown cells: tumor cells; blue cells: TIL; red stars: tumor-specific mutations. **(b)** Flow cytometric analysis of neo-antigen reactive T-cell populations in TIL of MDACCTIL2379. Top: neo-antigen reactive T-cell populations specific for mutant RASSF1 (left) and DHX33 (right). Percentages of pMHC double-positive cells within total CD8⁺ cells are indicated. Bottom: amino-acid sequences,

MHC-restriction and MHC-binding affinities for wild type (WT) and mutant (MT) peptides, as well as RNA expression levels in Fragments Per Kilobase of exon per Million fragments mapped (FPKM). **(c)** Flow cytometric analysis of mutant DHX33-specific T cells present in peripheral blood pre-therapy (left) and seven days post-therapy (right). Percentages of pMHC double-positive cells within total $CD8^+$ cells are indicated. **(d)** Flow cytometric analysis of neo-antigen reactive T-cell populations in TIL of NKIRTIL006. Top: neo-antigen reactive T-cell populations specific for mutant CDK4 (left), mutant GCN1L1 (middle), and mutant DNAH17 (right). Percentages of pMHC double-positive cells within total $CD8^+$ cells are indicated. Bottom: epitope characteristics as in Fig. 1B. **(e)** Functional activity of enriched TIL, analyzed by intracellular IFN-γ cytokine staining upon coculture with wild type and mutant peptide-loaded T2 cells. Data are presented as percentages of IFN-γ producing $CD8^+$ T cells. Bars represent means of triplicates plus standard deviation. **(f)** Functional activity of standard TIL and enriched TIL, analyzed by intracellular IFN-γ cytokine staining upon coculture with autologous (NKIRTIL006) melanoma, and two allogeneic HLA-A*02:01 matched (mel526, which is known to express the previously described $CDK4_{R24C}$ mutation) and mismatched (mel938) melanoma cell lines. Data are presented as percentages of IFN-γ producing $CD8^+$ T cells. Bars represent means of triplicates plus standard deviation. Data are representative of two independent experiments. Samples were compared using an unpaired two-sided Student's t-test (*** $P < 0.001$; NS, not significant).

To evaluate the potency of neo-antigen specific T cells in an in vivo setting, NSG mice were injected with tumor cells of patient NKIRTIL006, and either the autologous standard TIL product or the autologous enriched TIL product was administered once when tumors were palpable (Fig. 2A). Engraftment of $CD8^+$ T cells in peripheral blood of mice treated with standard TIL and enriched TIL was comparable, with a peak in T-cell frequencies at day 5 and a subsequent rapid decline (Fig. 2B). Importantly, the composition of the engrafted T-cell compartment was significantly different, with dominance of $GCN1L1_{L2330P}$ and $CDK4_{R24L}$ -specific T cells only seen in mice treated with enriched TIL (2% versus 85% mean combined $GCN1L1_{L2330P}$ and $CDK4_{R24L}$ reactivity at day 5, Fig. 2B). Strikingly, while a slight decrease in tumor growth was initially seen in both treatment groups, prolonged tumor control and survival was only observed in mice treated with enriched TIL (Fig. 2C and 2D). This superior activity of neo-antigen selective TIL is directly due to the higher number of these cells, rather than the removal of potentially inhibitory T-cell subsets, as shown by analysis of tumor growth of mice treated with the fraction of neo-antigen reactive cells present within the bulk TIL product (Fig. 2E). Interestingly, while in vivo retreatment had no effect on tumor outgrowth in two out of three mice previously treated with enriched TIL (Supplementary Fig. 2A), all recurring tumors still expressed MHC class I (Supplementary Fig. 2B) and were recognized efficiently in vitro (Supplementary Fig. 2C), suggesting that escape of antigen-loss variants did not occur.

Figure 2. Neo-antigen reactive TIL mediate superior tumor control over standard 'bulk' TIL in a mouse model of human melanoma. (a) In vivo set-up to compare tumor control upon treatment with standard TIL and TIL enriched for neo-antigen reactivity. Brown cells: tumor cells; blue cells: bulk TIL; red cells: neo-antigen specific TIL. **(b)** Flow cytometric analysis of tail vein-derived blood taken from mice treated with standard (n = 5, blue square) or enriched TIL (n = 5, red triangle), or from untreated control mice (n = 4, green circle) at the indicated time points post-TIL infusion (16 x 10^6 total cells per mouse administered i.v.). All mice received high-dose IL-2 (7.2 x 10^5 IU) twice daily for three days after TIL infusion. Left: percentage of human $CD8^+$ T cells of total live lymphocytes; middle: percentage of mutant $CDK4_{R24L}$ -specific T cells within the total $CD8^+$ T-cell population; right: percentage of mutant $GCN1L1_{L2330P}$ -specific T cells within the total $CD8^+$ T-cell population. Data are presented as mean ± s.d. There was no statistically significant difference between engraftment of total $CD8^+$ T cells from standard TIL and enriched TIL. Frequencies of neo-antigen specific cells were significantly higher in recipients of enriched TIL as compared to recipients of standard TIL at all time points ($P < 0.001$). **(c)** Tumor growth in mice treated with standard TIL or enriched TIL, or in untreated control mice. Data are presented as mean ± s.d. **(d)** Survival analysis of mice treated with standard TIL or enriched TIL, or of untreated control mice. Survival distribution was analyzed by log-rank test (standard vs. enriched $P < 0.005$). **(e)** Tumor growth in non-treated mice (n = 4, green circles), and in mice treated with standard TIL (n = 4, 10 x 10^6 cells per mouse, blue squares), neo-antigen enriched TIL (n = 5, 10 x 10^6 cells per mouse, red triangles), or an equivalent number of neo-antigen reactive TIL as present in the bulk TIL (n = 5, 2.72 x 10^5 cells per mouse, yellow triangles). In this setup, the standard TIL group and fraction TIL group received equal numbers (1.95 x 10^5) of neo-antigen reactive T cells. All mice received high-dose IL-2 (7.2 x 10^5 IU) twice daily for three days after TIL infusion. Data are presented as mean ± s.d. There was a statistically significant difference in tumor control from day 17 onward for neo-antigen enriched TIL vs. standard TIL ($P < 0.005$) and neo-antigen enriched TIL vs. fraction TIL ($P < 0.005$). At day 17, mice treated with standard TIL had significantly lower tumor burden compared to mice treated with fraction TIL ($P = 0.02$). Samples were compared using an unpaired two-sided Student's t-test. **(f)** Tumor growth in untreated control mice (n = 7, green circles), or in mice treated with standard TIL (n = 6, blue squares), neo-antigen enriched TIL (n = 5, red triangles), or C/G-antigen enriched TIL (n = 6, yellow triangles). All treated mice received 20 x 10^6 total cells i.v. Contribution of the aimed for antigen-specific T-cell population, as assessed by MHC multimer staining, was 37.5% for both recipients of C/G-antigen and neo-antigen enriched TIL. All mice received high-dose IL-2 (7.2 x 10^5 IU) twice daily for three days after infusion. Previously expanded TIL cultures were used, which were re-expanded (REP2) after enrichment to generate the TIL infusion products. Data are presented as mean ± s.d. There was a statistically significant difference in tumor control at day 14 for neo-antigen enriched TIL vs. standard TIL ($P = 0.02$) and neo-antigen enriched TIL vs. C/G-antigen enriched TIL ($P = 0.02$), but not for standard TIL vs. C/G-antigen enriched TIL ($P = 0.98$). Samples were compared using an unpaired two-sided Student's t-test. ➔

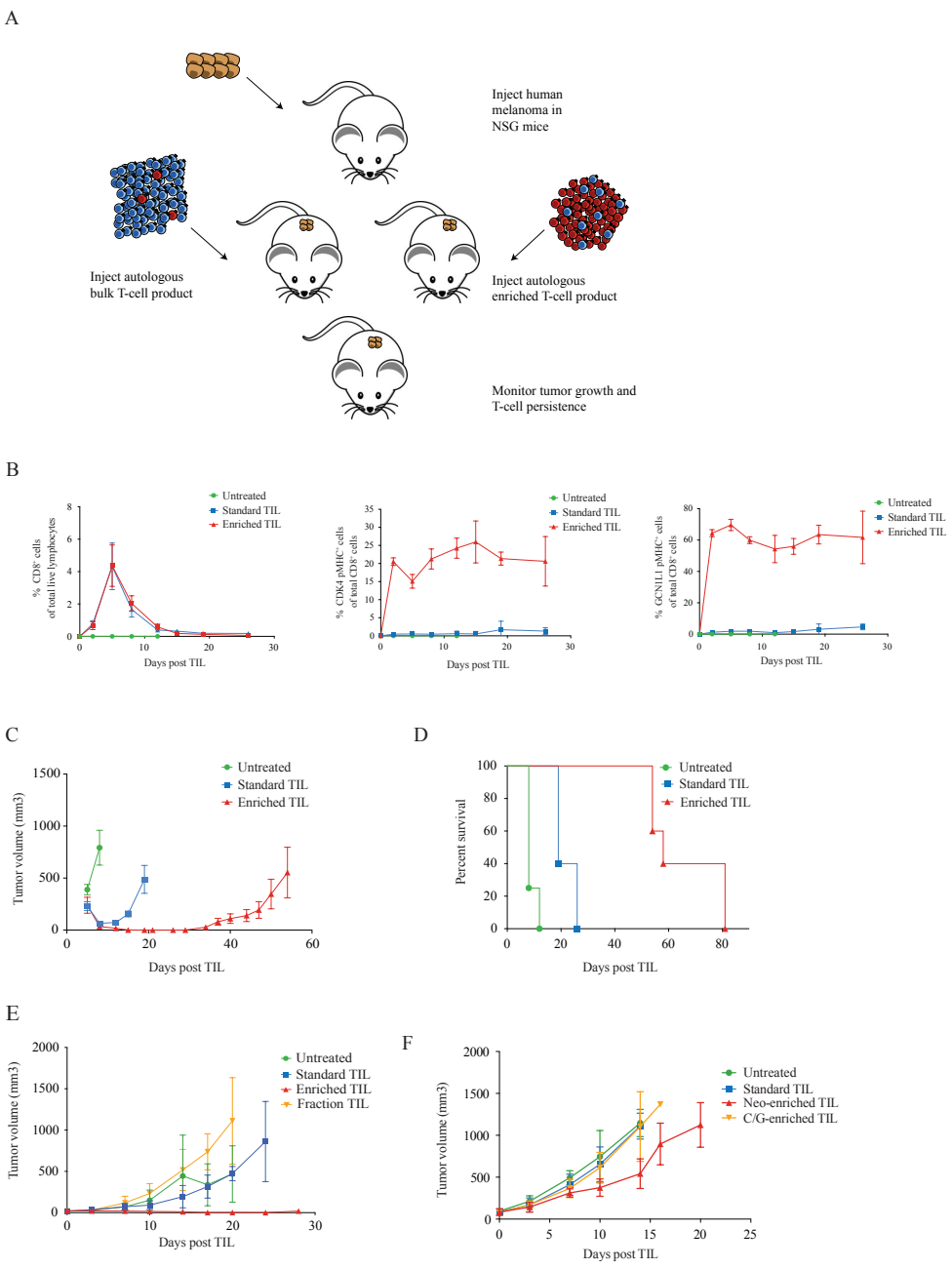
A
Inject human melanoma in NSG mice
Inject autologous bulk T-cell product
Inject autologous enriched T-cell product
Monitor tumor growth and T-cell persistence
B
Untreated
Standard TIL
Enriched TIL
% CD8+ cells of total live lymphocytes
% CDK4 pMHC+ cells of total CD8+ cells
% GCN1L1 pMHC+ cells of total CD8+ cells
Days post TIL
C
Tumor volume (mm3)
Days post TIL
D
Percent survival
Days post TIL
E
Fraction TIL
F
Neo-enriched TIL
C/G-enriched TIL

Next, we aimed to address whether TIL products enriched for reactivity against other classes of potentially relevant tumor rejection antigens could achieve a similar anti-tumor effect as TIL enriched for neo-antigen reactivity. Analysis of NKIRTIL006 by staining with a panel of HLA-A*02:01 multimers containing shared melanoma antigens had revealed the presence of T-cell reactivity against the Cancer/Germline (C/G) antigens MAGE-A10$_{GLY}$, MAGE-C2$_{LLF}$, MAGE-C2$_{VIW}$ and MACE-C2$_{ALK}$ (3.16%, 0.09%, 0.59% and 0.89% of CD8^{+} T cells, respectively)[20]. To analyze the potential value of these C/G-antigen reactive T-cell responses, we independently enriched TIL cultures for either neo-antigen (CDK4$_{R24L}$ and GCN1L1$_{L2330P}$) reactivity or C/G-antigen (MAGE-A10 and MAGE-C2) reactivity (Supplementary Fig. 3A). For both groups, the TIL cultures were again expanded after enrichment (necessary to obtain sufficient numbers of MAGE-A10/ MAGE-C2 enriched T cells from the low number of starting cells). Subsequently, frequencies of MHC multimer positive cells were adjusted to the same level for both groups (resulting in a combined frequency of either neo-antigen or C/G-antigen reactive T cells of 37.5%) and the C/G and neo-antigen specific T cell-enriched TIL products were used for treatment of NSG mice carrying established autologous melanoma. Following infusion, a similar engraftment of TIL was observed across all treatment groups (Supplementary Fig. 3B). While overall anti-tumor activity was lower than in experiments using TIL expanded only a single time, also in this setting a significant difference in tumor outgrowth between mice treated with standard TIL and neo-antigen enriched TIL was observed ($P < 0.05$). In contrast, infusion of C/G-antigen enriched TIL was not superior over treatment with standard TIL ($P = 0.98$, Fig. 2F). Furthermore, we observed a significant difference in tumor outgrowth between mice treated with neo-antigen enriched TIL as compared to mice treated with C/G-antigen enriched TIL ($P = 0.02$, Fig. 2F), indicative of a qualitative difference between epitope classes targeted by TIL therapy in this patient. However, the relative fitness of the enriched cell populations could be a major confounder for their tumoricidal potential. To enable a full qualitative comparison between TCR specificities, we sequenced the genes of each respective TCR alpha/beta chain, cloned them into a retroviral vector for expression on peripheral blood mononuclear cells (PBMCs) (Supplementary Fig. 4A) and confirmed their reactivity against the autologous tumor cell line (Supplementary Fig. 4B). We then treated tumor-bearing NSG mice with either a mixture of the two neo-antigen reactive TCR transduced PBMCs or a mixture of the four C/G antigen reactive TCR transduced PBCMs or with non transduced PBMCs as a control (Supplementary Fig. 4C). Upon infusion, all mice treated with neo-antigen reactive TCRs experienced complete tumor control (Fig. 3A), without late recurrence as was initially observed in the TIL treatment setting. Mice treated with C/G antigen reactive TCRs experienced some initial tumor control but eventually all mice were sacrificed because of tumor recurrence (Fig. 3B). To dissect differences with respect to tumor clearance within the group of neo-antigen reactive TCRs, we treated two additional groups with either CDK4 or GCN1L1 reactive

PBMCs. To our surprise, only mice treated with the CDK4 TCR transduced PBCMs completely rejected the tumor (Fig. 3C). This may be a TCR intrinsic feature, as a subsequent k_{off}-rate assay[21] showed a significant difference in binding affinity of the CDK4 TCR in comparison with the GCN1L1 TCR and two of the four MAGE TCRs that we were able to test (Fig. 3D). These data indicate that within the group of neo-antigen reactive T cells there still may be heterogeneity in, although this is certainly not limited to, the quality of the T-cell response. Validation of TCR binding affinity may thus provide important information on tumor-control efficacy of reconstructed autologous TCRs for adoptive cell therapy approaches.

This report provides both indirect and direct support for the (pre-) clinical relevance of neo-antigen reactive T-cell populations in two melanoma patients. It is, however, important to point out that neo-antigen specific $CD8^+$ T-cell reactivity will not be a dominant factor in all patients that respond to immunotherapy. For instance, in tumors with a more modest mutational load, T-cell reactivity against non-mutant antigens could be a more critical factor, for the simple reason that the available repertoire of mutant antigens is limited. The observation that the clinical activity of recently developed immunotherapeutics is particularly pronounced in tumors with high mutational loads suggests that at least for these tumors an increased focus on patient-specific mutated antigens is warranted[22-25]. Clinical studies performed by Rosenberg and colleagues have already demonstrated that neo-antigen reactive T-cell populations enriched from clinical TIL products can exert profound clinical effects and that such a procedure is feasible at a clinical-grade level. Unfortunately, data from such trials will only provide correlative evidence for the involvement of T cells targeting neo-antigens, whereas the combination of our in vivo model system and T-cell receptor affinity assessment makes it possible to compare the quality of distinct T-cell responses targeting putative tumor-rejection antigens in a direct manner. As mentioned earlier, the differences we observed in tumor-clearance efficacy are likely not limited to TCR affinity alone but can also be related to whether a driver or a passenger mutation is being targeted or to differences in antigen expression levels. Furthermore, analyses on additional patients are required to gain insights in the tumoricidal fraction of the total neo-antigen reactive T-cell pool. Ultimately, mouse model systems might still be required as a learning strategy for the effects of hierarchical targeting of neo-antigens[26] before we will be able to discern which form the more superior targets in obtaining tumor control in each individual patient.

In summary, ongoing developments in next-generation sequencing platforms and in silico prediction algorithms have made it feasible to identify patient-specific mutant epitopes within individual patients, and should make it feasible to enhance T-cell responses against such epitopes in a therapeutically relevant time frame in future studies.

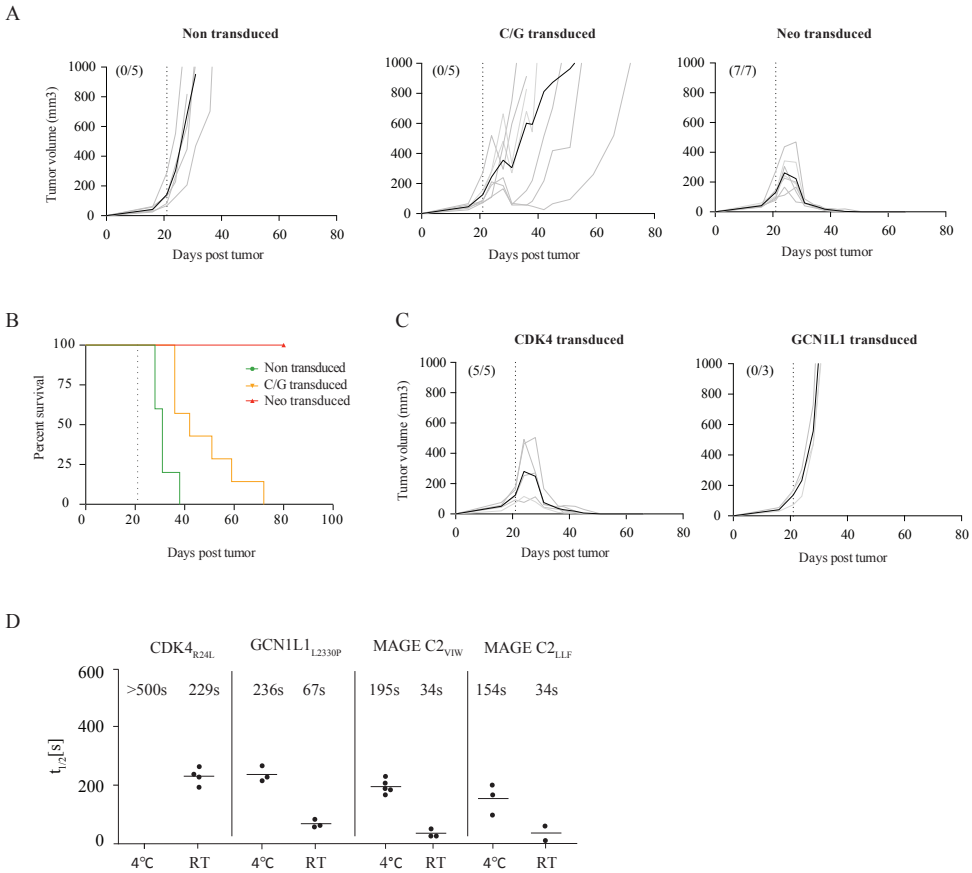

Figure 3. (a) Tumor growth in mice treated with control non transduced T cells (left), C/G TCR transduced T cells (middle) or neo TCR transduced T cells (right). Graphs show tumor growth of each individual mouse (grey line) and the average of the group (black line). Dotted line indicates time-point of T-cell infusion. Number of complete responders per group is indicated between brackets. Mice received 1e6 total $CD8^+TCR^+$ T cells. (b) Survival analysis per group is shown. (c) Tumor growth in mice treated with either $CD8^+CDK4^+$ T cells or $CD8^+GCN1L1^+$ T cells. **(d)** k_{off}-rate assay was performed at 4 °C or room temperature (RT) for 4 out of 6 TCRs. TCR staining with streptamers was not detectable for MAGE-$C2_{ALK}$ and MAGE-$A10_{GLY}$ TCRs.

METHODS

Patient material and cell cultures. Material was obtained from patients (NKITRIL006 and MDACCTIL2379) with progressive stage IV melanoma after informed consent had been signed and with approval of the local medical ethical authorities. MDACCTIL2369 was treated in a phase II clinical trial study of TIL therapy (NCT00338377) at the MD Anderson Cancer Center under study protocol 2004-006910. Response evaluation was performed

according to standard RECIST criteria as well as irRC[27]. TIL and tumor cell line cultures from both institutes were established from resection material according to identical protocols. Expansion of TIL cultures was performed according to a Rapid Expansion Protocol[10]. Cells were cryopreserved in 10 % DMSO and stored in liquid N2.

Exome sequencing and detection of somatic mutations. Genomic DNA was extracted from cell pellets using the QIAGEN DNeasy purification kit. Libraries of genomic DNA were prepared using the Illumina Paired-End Sample Prep kit following the manufacturer's guidelines. Resulting gDNA libraries were enriched for exonic sequences as described previously using the Agilent Sure Select Human All Exon 50Mb target enrichment system[28]. Sequencing was performed on an Illumina HiSeq DNA Analyzer (75bp paired-end reads), according to the manufacturer's instructions. Reads were aligned to the human reference genome (NCBI Build 37) using the Burrows-Wheeler Aligner algorithm[29]. Unmapped reads, read mapping outside the targeted region and PCR-derived duplicates were excluded from further analyses.

To call substitutions and indels, the CAVEMAN and PINDEL algorithms were used, respectively, as implemented by the Cancer Genome Project[30]. The precision of substitution calling was determined by re-sequencing DNA from one sample (NKIRTIL006) at the NKI Genomics Core Facility, using the same sequencing platform but calling substitutions using Somatic SNIPER31. Indels were validated by manual inspection.

RNA sequencing and gene expression. RNA was isolated using the QIAGEN RNeasy purification kit. Poly-A selected RNA libraries were then prepared, using the TruSeq RNA library protocol (Illumina, San Diego, CA, USA), and the resulting libraries were sequenced on an Illumina HiSeq2000 using 75bp paired-end reads. Reads were aligned using Tophat (version 1.3.3)[32]. Expression values were calculated as FPKM using Cufflinks (version 1.0.2)[33].

Epitope Predictions. Amino acid stretches of 39 aa with the mutated amino acid at position 20 were used to perform predictions of proteasomal cleavage (NetChop[34],) and MHC class I binding (NetMHC3.2 and NetMHCpan2.4[35,36]). For those mutations located within 20 amino acids from the N- or C-terminus of the protein, shorter fragments were used. The following peptides were selected; 1) those epitopes that contain the mutated amino acid; and 2) derived from genes with FPKM values > 0 (as there is little known about the importance of RNA expression levels, this low threshold was chosen); and 3) with a predicted C terminal cleavage probability of > 0.5; and 4) with predicted binding affinities of: < 8,500nM for the HLA-A*01:01 allele, <3,100 nM for the HLA-A*23:01 allele, <13,000 nM for the HLA-B*55:01 allele, < 1,000nM for the HLA-A*02:01 allele, and <600 nM for the HLA-B*15:01 allele. The latter cut-offs were chosen such that per 100 mutations, a total of 35 peptides/allele (a

sum of 9-, 10- and 11-mers) are included in the screen for each allele, a number based on predictions using a model set of mutations.

Generation of pMHC multimers. Panels of pMHC multimers were generated by coupling each pMHC complex to a defined combination of two out of eight different fluorescent streptavidin (SA) conjugates (Invitrogen, Carlsbad, CA, USA). For each 10 µl of pMHC monomer (100 µg ml^{-1}), the following amount of SA-conjugates were utilized: 1.5 µl SA-QD605, 1.0 µl SA-QD625, 1.5 µl SA-QD655, 1.5 µl SA-QD705, 1.0 µl SA-QD800, 0.9 µl SA-PE (1 mg ml^{-1}) and 0.6 µl SA-APC (1 mg ml^{-1}). Mixtures were incubated on ice for 30 min. NaN3 (0.02% wt/vol) and an excess of D-biotin (26.4 mM, Sigma-Aldrich, St. Louis, MO, USA) were added, the latter to block residual binding sites.

T-cell staining with pMHC multimers. Thawed cells were incubated with 25 U/ml benzonase (Novagen, EMD Millipore, Billerica, MA, USA) for 1 hr at 37 °C. For T-cell staining, the following amounts of fluorescently labeled pMHC complexes were pooled together for combinatorial coding: 1 µl for each PE-labeled pMHC complex, 2 µl for each APC-labeled pMHC complex, 3 µl for each QD605-labeled pMHC complex, 2 µl for each QD625-labeled pMHC complex, 2 µl for each QD655-labeled pMHC complex, 4 µl for each QD705-labeled pMHC complex, 4 µl for each QD800-labeled pMHC complex, and 3 µl for each PE-Cy7-labeled pMHC complex. Cells were incubated in a total volume of 135 µl at 37 °C for 15 min. 2 µl anti-CD8-FITC (clone SK1, BD Bioscience, San Diego, CA, USA), 1 µl anti-CD4-AF700 (clone S3.5, Invitrogen, Carlsbad, CA, USA) and 0.5 µl LIVE⁄DEAD® Fixable Violet Dead Cell Stain Kit (Invitrogen, Carlsbad, CA, USA) was subsequently added, and cells were incubated on ice for 30 min. Prior to flow cytometric analysis, cells were washed twice in 200 µl FACS buffer, 1500 RPM, 3 minutes.

Flow cytometry. Data acquisition of T-cell screens was performed on an LSR-II flow cytometer (BD Bioscience, San Diego, CA, USA) with FacsDiva software, utilizing the following eleven color instrument setting: UV laser (355 nm): QD605, 595LP, 605/12; QD705, 685LP, 710/50; QD800, 750LP, 780/60. Violet laser (405 nm): QD625, 610LP, 625/20; QD655, 635LP, 655/8. Blue laser (488 nm): FITC, 505LP, 525/50. Yellow-green laser (561 nm): PE, 585/15; PE-Cy7, 750LP, 780/60. Red laser (640 nm): APC, 670/14; AF700, 685LP, 710/50; IR-Dye, 750LP, 780/60. To identify antigen-specific T cells, the following gating strategy was used. 1) Selection of live (IR-dye negative) single cell lymphocytes (FSC-W/H low, SSC-W/H low, FSC/SSC-A). 2) Selection of anti-CD8-$FITC^+$ and 'dump' (anti-CD4) negative cells. 3) Selection of $CD8^+$ T cells that were positive in two and only two MHC multimer channels.

T-cell enrichment. Enrichments were performed using MHC-exchange molecules equipped with a strep-tag III19. Complexes were exposed to 366 nm UV light (CAMAG, The Netherlands) at 4 °C in the presence of a rescue peptide. MHC streptamers were generated by conjugating the resulting exchange reaction to magnetic microbeads, according to the manufacturer's protocol (IBA, Göttingen, Germany). T cells were labeled using 1 µg of MHC streptamer per $1x10^7$ cells. Antigen-specific cells were positively selected using LS columns (Miltenyi Biotec, Bergisch Gladbach, Germany). After enrichment, cells were incubated with 10 mM D-biotin (IBA, Göttingen, Germany) to dissociate MHC reagents.

TCR gene expression on PBMCs. TCR genes from single-cell sorted T-cell clones were determined by high-throughput deep-sequencing using a previously published method and subsequently cloned into a retroviral vector construct37. Transduction efficiency was determined by pMHC multimer and murine constant domain staining (anti-mouse-beta-chain-PE, clone H57-597, BD Pharmingen, San Diego, CA, USA).

K_{off}-rate assay. TCR binding affinity was assessed in a k_{off}-rate assay as previously described[21]. In short, transduced T cells were stained with pMHC Alexa488 and *Strep*-Tactin APC beads (Superflow, 50 % suspension, IBA). The decay of fluorescence signal was measured after the addition of D-biotin using real-time fluorescence microscopy, followed by the decay of fluorescence signal reflecting the dissociation of monomeric MHC molecules. k_{off}-rate and half-life time ($t_{½}$) values were calculated using MetaMorph Offline image analysis software (Molecular Devices).

Functional analyses. To determine antigen reactivity (analyses performed in triplicate), indicated effector cells were cultured at a 1:1 ratio with target cells for 5 hr at 37 °C and 5% CO2 (BD Pharmingen, San Diego, CA, USA). Target cell lines were either autologous (NKIRTIL006), HLA-A*02:01 matched (mel526), HLA-A*02:01 mismatched (mel938) or peptide-loaded T2 cells. Peptide loading was performed for 1 hr at 37 °C and 5% CO2 and cells were washed twice after incubation. After a 5 hr coculture, cells were stained with anti-CD8 PerCP-Cy5.5 (clone SK-1, BD Pharmingen, San Diego, CA, USA) and anti-CD3 FITC (clone SK7, BD Pharmingen, San Diego, CA, USA), fixed with Cytofix/Cytoperm according to the manufacturer's guidelines (BD Bioscience, San Diego, CA, USA), and stained for intracellular IFN-γ expression using anti-IFN-γ APC (clone B27, BD Pharmingen, San Diego, CA, USA). Samples were measured on a Fortessa flow cytometer (BD Bioscience, San Diego, CA, USA) with FacsDiva software and analyzed using FlowJo software version (version 9.4, Treestar Inc., San Carlos, CA, USA).

Chromium release assays were performed by labeling target cells for 1 hr at 37 °C with 100 mCi (3.7 MBq) ^{51}Cr (Amersham, Ghent, Belgium). Labeled target cells were washed three times with RPMI 1640 medium containing 5% FCS and were then incubated with effector

cells at the indicated ratios for 4 hr at 37 °C and 5% CO2 in 200 µL medium. Maximal and spontaneous release was determined by the addition of 1 % Triton X-100 (Sigma-Aldrich, St. Louis, MO, USA) or addition of medium alone, respectively. ^{51}Cr release was determined by transfer of 50 µl of supernatant to a Lumaplate (Perkin-Elmer, Waltham, MA, USA) and measurement in an automatic counter (Topcount, Perkin-Elmer). The percentage of specific release was calculated as: ((cpm experimental release – cpm spontaneous)/(cpm maximal – cpm spontaneous)) x 100.

In vivo model. NSG mice (The Jackson Laboratory, Bar Harbor, ME, USA) were housed in the Experimental Animal Department of The Netherlands Cancer Institute. All mouse experiments were performed in accordance with institutional and national guidelines and were approved by the Experimental Animal Committee (DEC) of The Netherlands Cancer Institute.

Female mice of at least 8 weeks old were challenged by subcutaneous injection of 1 x 10^6 tumor cells embedded in matrigel (BD Bioscience, San Diego, CA, USA) in the flank. When tumors were palpable, mice were ranked by tumor size and randomized to ensure equal average tumor size per group with at least four mice per experimental group (no power calculations were performed). Subsequently, the indicated numbers of autologous T cells were injected intravenously, immediately followed by high-dose (7.2 x 10^5 IU) IL-2 (Proleukin, Novartis) intraperitoneally twice daily for three consecutive days. Control mice received no T cells or non transduced PBMCs. Tumors were measured twice per week by a researcher blinded to the experimental condition, using a digital caliper. Animals were sacrificed when tumors exceeded 15 mm in any dimension or when the average of two dimensions was higher than 12 mm. Blood samples were taken from the tail vein twice weekly. Recurring tumors were enzymatically digested and stained with anti-HLA-ABC-PE (clone G46-2.6, BD Pharmingen, San Diego, CA, USA). Immune monitoring was performed on a Fortessa flow-cytometer (BD Bioscience, San Diego, CA, USA).

Statistical analysis. Samples were compared using an unpaired, two-sided Student's t-test, unless specified otherwise. P-values <0.05 were considered statistically significant.

Data deposition. DNA and RNA sequencing data are deposited: EGAD00001000243 (https://www.ebi.ac.uk/ega/studies/EGAS00001000216) and EGAD00001000325 (https://www.ebi.ac.uk/ega/studies/EGAS00001000251). Data on MDACCTIL2379 can be found under PD13414a, PD13414b and PR13414a. Data on NKIRTIL006 can be found under PD9029a, PD9029b and PR9029a.

ACKNOWLEDGEMENTS

The authors would like to thank D. El Atmioui and H. Hilkmann of the Netherlands Cancer Institute Peptide Synthesis facility for technical support. We thank A. Velds and R. Kerkhoven for support on sequence analyses, H. van Tinteren for support with statistical analyses, C. Kesmir for advice on bio-informatics analyses, and R. Mezzadra for technical assistance. We would like to thank C. Linnemann and G. Bendle for critical reading of the manuscript and members of the Schumacher and Haanen laboratories for useful discussions. S.B. receives a Wellcome Trust Research Training Fellowship for Clinicians. This work was partly supported by the NIH, NCI grant R01 CA111999 and accompanying ARRA supplement to P.H. and the Dr. Miriam and Sheldon G. Adelson Medical Research Foundation award titled “Interactive program to identify predictive biomarkers in TIL therapy” to L.G.R. and C.B. This work was supported by Dutch Cancer Society grant KWF 2012-5463 to T.N.M.S., and by a Stand Up To Cancer–Cancer Research Institute Immunology Translational Cancer Research Grant to T.N.M.S. SU2C is a program of the Entertainment Industry Foundation administered by the American Association for Cancer Research.

AUTHOR CONTRIBUTIONS

S.K. and L.B. designed, performed, analyzed and interpreted experiments, and wrote the paper. M.v.B. performed bio-informatics analyses and epitope predictions. M.v.B., N.v.R. and D.P. performed and analyzed T-cell neo-antigen screens. M.T. and L.J.A.D. synthesized MHC reagents. S.M. and L.F. provided technical assistance. K.K., L.B. and D.S.P. developed patient-derived xenograft systems for human melanoma. S.B. and M.R.S. designed, performed and interpreted sequencing experiments and provided bio-informatics support. L.G. designed MHC streptamers, B.W. and D.H.B. performed and interpreted k_{off}-rate experiments and B.H. contributed to the streptamer enrichment technology. C.B., L.G.R., C.U.B., P.H. and J.B.A.G.H. were involved in clinical trials, patient material collection and interpreted patient data. P.K. designed and performed T-cell neo-antigen screens, analyzed and interpreted data, and provided manuscript corrections. T.N.M.S. supervised the project, designed and interpreted all experiments, and wrote the paper.

Competing financial interests. L.G. is shareholder and co-founder of Stage Cell therapeutics, which produces the MHC streptamers used in this project. All other authors declare no competing financial interest.

Supplementary Figure 1. Enrichment and functional analysis of neo-antigen reactive T cells in bulk melanoma TIL culture. **(a)** Change in tumor burden of patient MDACCTIL2379 relative to that at start of TIL therapy (1 x 10^{11} cells plus high-dose IL-2) is depicted. Measurements were performed on a target lesion in the right long using computed-tomography (CT) scanning images and reported according to immune-related response criteria (irRC) and RECIST. **(b)** Mutational profiles of patient MDACCTIL2379 (left) and NKIRTIL006 (right). Total number of somatic mutations is indicated. **(c)** Engraftment of mutant DHX33-specific T cells in peripheral blood of patient MDACCTIL2379 upon TIL therapy, as measured by MHC multimer combinatorial coding. **(d)** MHC multimer-based enrichment of neo-antigen reactive TIL from bulk melanoma TIL culture of patient NKIRTIL006. Left: pre-enrichment; Middle: post-enrichment; Right: post-REP. Data depict the percentage of pMHC double-positive cells within the total $CD8^+$ T-cell population. Combined purity of TIL product (in percentages) is depicted below. **(e)** Chromium-release assay to measure cytolytic activity against autologous tumor cells of either standard TIL or neo-antigen enriched TIL at the indicated effector to target (E:T) ratios. Data are presented as means of triplicates ± s.d. Samples were compared using an unpaired two-sided Student's t-test (*P<0.05, **P<0.01). ➔

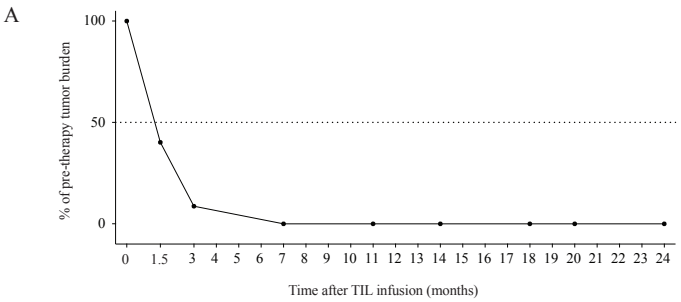
A
100
50
0
% of pre-therapy tumor burden
0 1.5 3 4 5 6 7 8 9 10 11 12 13 14 15 16 17 18 19 20 21 22 23 24
Time after TIL infusion (months)

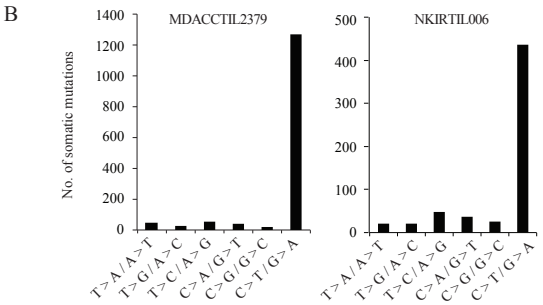
B
MDACCTIL2379
NKIRTIL006
No. of somatic mutations
1400
1200
1000
800
600
400
200
0
500
400
300
200
100
0
T>A/A>T
T>G/A>C
T>C/A>G
C>A/G>T
C>G/G>C
C>T/G>A

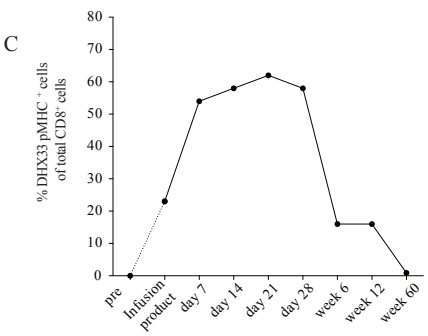
C
% DHX33 pMHC+ cells of total CD8+ cells
80
70
60
50
40
30
20
10
0
pre
Infusion product
day 7
day 14
day 21
day 28
week 6
week 12
week 60

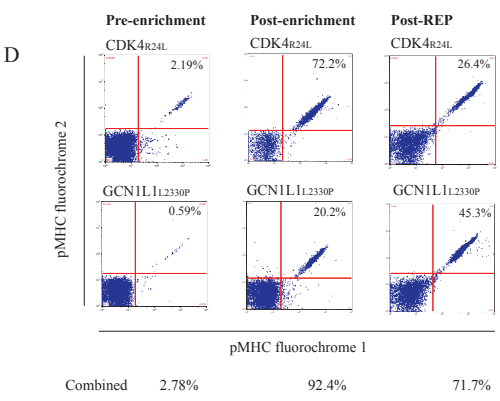
D
Pre-enrichment
Post-enrichment
Post-REP
CDK4R24L
2.19%
72.2%
26.4%
GCN1L1L2330P
0.59%
20.2%
45.3%
pMHC fluorochrome 2
pMHC fluorochrome 1
Combined 2.78% 92.4% 71.7%

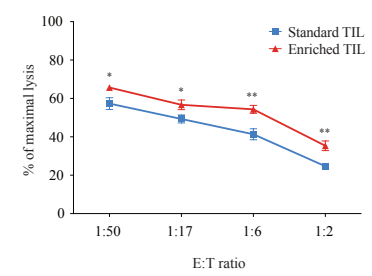
E
100
80
60
40
20
0
% of maximal lysis
Standard TIL
Enriched TIL
*
*
**
**
1:50
1:17
1:6
1:2
E:T ratio

Supplementary Figure 2. Disease recurrence in the absence of immune editing. (a) Tumor growth in individual untreated control mice (n = 4, green), or in mice treated (first dotted vertical line) with standard TIL (n = 4, blue), neo-antigen enriched TIL (n = 5, red), or fraction TIL (n = 5, yellow). Three recipients of neo-antigen enriched TIL group were retreated (TIL x2, second dotted vertical line) with neo-antigen enriched TIL (10×10^6 total cells per mouse) and high-dose IL-2 (7.2×10^5 IU) twice daily for three days at the time of tumor recurrence (day 51). The remaining two mice received no additional infusion of TIL but did receive high-dose IL-2 (7.2×10^5 IU) twice daily for three days at the time of tumor recurrence (day 85). **(b)** Recurring tumors were analyzed for expression of MHC class I by flow cytometry. Overlays of histograms are shown, grey filled area are unstained control cells. MFI denotes median fluorescence intensity. TIL x1 denotes mice that were treated with a single TIL infusion and had complete tumor regression until day 80; TIL x2 (R) denotes the mouse that, after initial tumor control received a second TIL infusion at day 51 and experienced complete regression until day 80; TIL x2 (NR) denotes mice that, after initial tumor control, received a second TIL infusion at day 51 to which they did not respond. **(c)** Analysis of (neo-) antigen presentation by recurring tumors, as measured by intracellular IFN-γ cytokine staining of standard TIL and enriched TIL upon coculture with tumors from control mice, or mice treated with standard TIL or neo-antigen enriched TIL. Data are presented as percentages of IFN-γ producing $CD8^+$ T cells, black lines indicate mean values. ➔

A

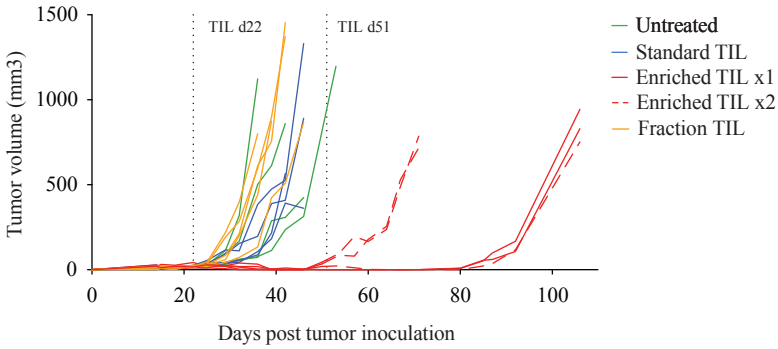

B

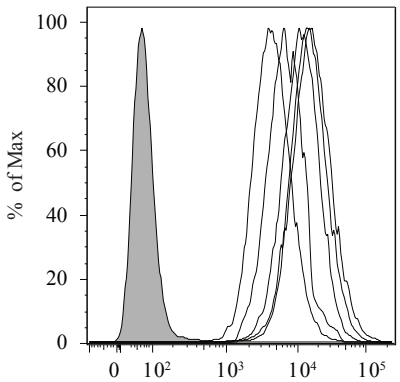

Mouse	MFI MHC class I
Enriched TIL X1	4372
Enriched TIL X1	6892
Enriched TIL x2 (R)	11687
Enriched TIL x2 (NR)	14873
Enriched TIL x2 (NR)	16738

C

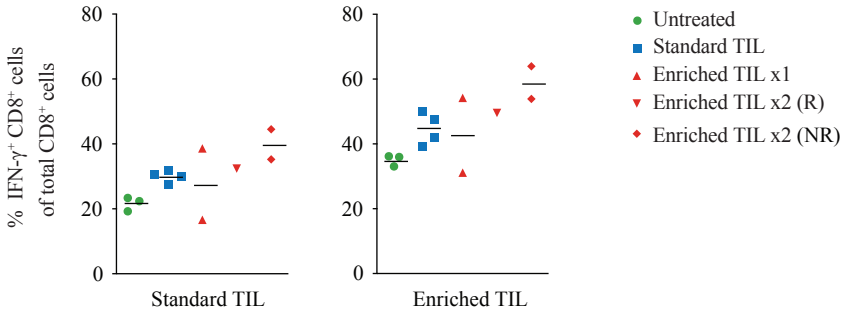

A

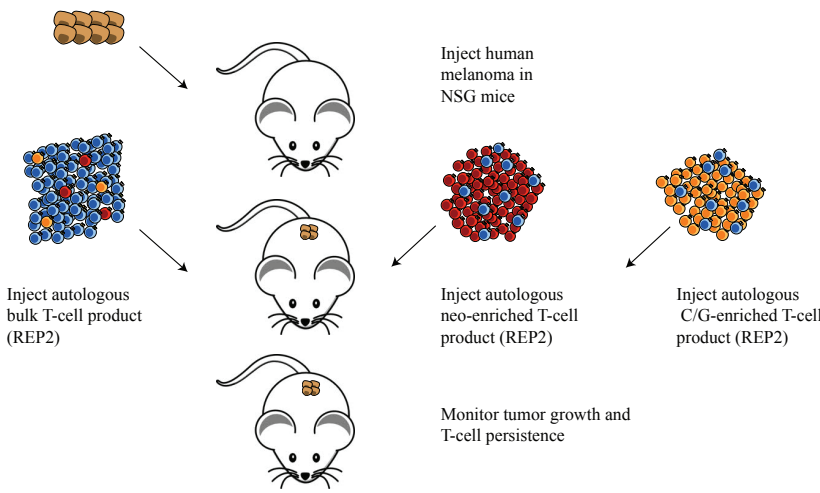

B

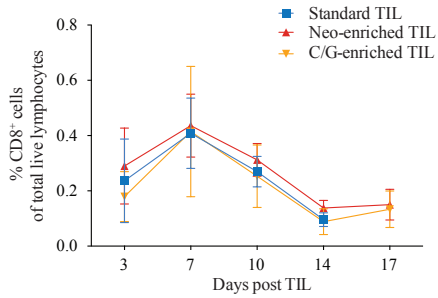

Supplementary Figure 3. Comparison of neo-antigen enriched T-cell product with C/G antigen enriched T-cell product. (a) In vivo set-up to compare tumor control upon treatment with standard TIL, neo-antigen enriched TIL and C/G-antigen enriched TIL. Brown cells: tumor cells; blue cells: bulk TIL; red cells: neo-antigen specific TIL; yellow cells: C/G-antigen specific TIL. For this experiment, previously expanded TIL cultures were enriched and re-expanded (REP2) to generate the TIL infusion products. **(b)** Flow cytometric analysis of tail vein-derived blood taken from untreated control mice (n = 7, green circles), or mice treated with standard TIL (n = 6, blue squares), neo-antigen enriched TIL (n = 5, red triangles), or C/G-antigen enriched TIL (n = 6, yellow triangles). All treated mice received 20 x 10^6 total cells i.v. plus high-dose IL-2 (7.2 x 10^5 IU) twice daily for three days. Numbers depict the percentage human $CD8^+$ T cells of total live lymphocytes. There was no statistically significant difference between engraftment of total $CD8^+$ T cells between all treatment groups. Data are presented as mean ± s.d. Samples were compared using an unpaired two-sided Student's t-test.

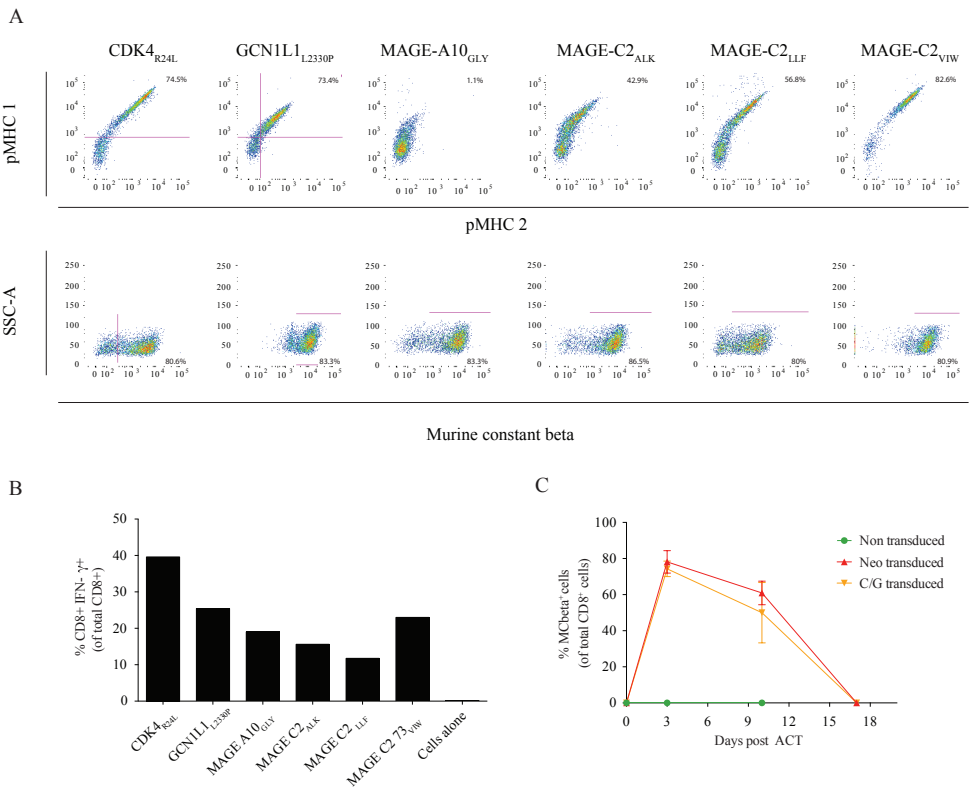

Supplementary Figure 4. Comparative analysis of isolated TCRs. (a) Transduction efficiency of each indicated TCR is shown by pMHC multimer staining (upper panel) or Murine constant domain staining (lower panel). **(b)** Reactivity of transduced T-cell cultures was determined by measuring intracellular IFN- γ cytokine staining upon coculture with the autologous tumor cell line. **(c)** Flow cytometric analysis of tail vein-derived blood from mice treated with non transduced (green circles), neo TCR transduced (red triangles) or C/G TCR transduced T cells (yellow triangles).

REFERENCES

1. Alexandrov, L.B.*, et al.* Signatures of mutational processes in human cancer. *Nature* **500**, 415-421 (2013).
2. Vogelstein, B.*, et al.* Cancer genome landscapes. *Science* **339**, 1546-1558 (2013).
3. Segal, N.H.*, et al.* Epitope landscape in breast and colorectal cancer. *Cancer Res* **68**, 889-892 (2008).
4. Govindan, R.*, et al.* Genomic landscape of non-small cell lung cancer in smokers and never-smokers. *Cell* **150**, 1121-1134 (2012).
5. Linnemann, C.*, et al.* High-throughput epitope discovery reveals frequent recognition of neo-antigens by $CD4^+$ T cells in human melanoma. *Nat Med* **21**, 81-85 (2015).
6. Lennerz, V.*, et al.* The response of autologous T cells to a human melanoma is dominated by mutated neoantigens. *Proc Natl Acad Sci U S A* **102**, 16013-16018 (2005).
7. van Rooij, N.*, et al.* Tumor exome analysis reveals neoantigen-specific T-cell reactivity in an ipilimumab-responsive melanoma. *J Clin Oncol* **31**, e439-442 (2013).
8. Robbins, P.F.*, et al.* Mining exomic sequencing data to identify mutated antigens recognized by adoptively transferred tumor-reactive T cells. *Nat Med* **19**, 747-752 (2013).
9. Lu, Y.C.*, et al.* Mutated PPP1R3B is recognized by T cells used to treat a melanoma patient who experienced a durable complete tumor regression. *J Immunol* **190**, 6034-6042 (2013).
10. Radvanyi, L.G.*, et al.* Specific lymphocyte subsets predict response to adoptive cell therapy using expanded autologous tumor-infiltrating lymphocytes in metastatic melanoma patients. *Clin Cancer Res* **18**, 6758-6770 (2012).
11. Wolfel, T.*, et al.* A p16INK4a-insensitive CDK4 mutant targeted by cytolytic T lymphocytes in a human melanoma. *Science* **269**, 1281-1284 (1995).
12. Coulie, P.G.*, et al.* A mutated intron sequence codes for an antigenic peptide recognized by cytolytic T lymphocytes on a human melanoma. *Proc Natl Acad Sci U S A* **92**, 7976-7980 (1995).
13. Robbins, P.F.*, et al.* A mutated beta-catenin gene encodes a melanoma-specific antigen recognized by tumor infiltrating lymphocytes. *J Exp Med* **183**, 1185-1192 (1996).
14. Tran, E.*, et al.* Cancer Immunotherapy Based on Mutation-Specific $CD4^+$ T Cells in a Patient with Epithelial Cancer. *Science* **344**, 641-645 (2014).
15. Rodenko, B.*, et al.* Generation of peptide-MHC class I complexes through UV-mediated ligand exchange. *Nat Protoc* **1**, 1120-1132 (2006).
16. Toebes, M.*, et al.* Design and use of conditional MHC class I ligands. *Nat Med* **12**, 246-251 (2006).
17. Hadrup, S.R.*, et al.* Parallel detection of antigen-specific T-cell responses by multidimensional encoding of MHC multimers. *Nat Methods* **6**, 520-526 (2009).
18. Lu, Y.C.*, et al.* Efficient identification of mutated cancer antigens recognized by T cells associated with durable tumor regressions. *Clin Cancer Res* **20**, 3401-3410 (2014).
19. Neudorfer, J.*, et al.* Reversible HLA multimers (Streptamers) for the isolation of human cytotoxic T lymphocytes functionally active against tumor- and virus-derived antigens. *J Immunol Methods* **320**, 119-131 (2007).
20. Kvistborg, P.*, et al.* TIL therapy broadens the tumor-reactive $CD8(^+)$ T cell compartment in melanoma patients. *Oncoimmunology* **1**, 409-418 (2012).
21. Nauerth, M.*, et al.* TCR-ligand koff rate correlates with the protective capacity of antigen-specific $CD8^+$ T cells for adoptive transfer. *Sci Transl Med* **5**, 192ra187 (2013).
22. Champiat, S., *et al.* Exomics and immunogenics: Bridging mutational load and immune checkpoints efficacy. *Oncoimmunology* **3**, e27817 (2014).

23. Le, D.T*., et al.* PD-1 Blockade in Tumors with Mismatch-Repair Deficiency. *N Engl J Med* **372**, 2509-2520 (2015).
24. Rizvi, N.A., *et al.* Mutational landscape determines sensitivity to PD-1 blockade in non–small cell lung cancer. *Science* **348**, 124-128 (2015).
25. Snyder, A*., et al.* Genetic Basis for Clinical Response to CTLA-4 Blockade in Melanoma. *N Engl J Med* **371**, 2189-2199 (2014).
26. Kreiter, S*., et al.* Mutant MHC class II epitopes drive therapeutic immune responses to cancer. *Nature* **520**, 692-696 (2015).
27. Wolchok, J.D*., et al.* Guidelines for the evaluation of immune therapy activity in solid tumors: immune-related response criteria. *Clin Cancer Res* **15**, 7412-7420 (2009).
28. Varela, I*., et al.* Exome sequencing identifies frequent mutation of the SWI/SNF complex gene PBRM1 in renal carcinoma. *Nature* **469**, 539-542 (2011).
29. Li, H. & Durbin, R. Fast and accurate long-read alignment with Burrows-Wheeler transform. *Bioinformatics* **26**, 589-595 (2010).
30. Behjati, S*., et al.* Recurrent PTPRB and PLCG1 mutations in angiosarcoma. *Nat Genet* **46**, 376-379 (2014).
31. Larson, D.E*., et al.* SomaticSniper: identification of somatic point mutations in whole genome sequencing data. *Bioinformatics* **28**, 311-317 (2012).
32. Trapnell, C., *et al.* TopHat: discovering splice junctions with RNA-Seq. *Bioinformatics* **25**, 1105-1111 (2009).
33. Trapnell, C*., et al.* Transcript assembly and quantification by RNA-Seq reveals unannotated transcripts and isoform switching during cell differentiation. *Nat Biotechnol* **28**, 511-515 (2010).
34. Nielsen, M., Lundegaard, C., Lund, O. & Kesmir, C. The role of the proteasome in generating cytotoxic T-cell epitopes: insights obtained from improved predictions of proteasomal cleavage. *Immunogenetics* **57**, 33-41 (2005).
35. Lundegaard, C*., et al.* NetMHC-3.0: accurate web accessible predictions of human, mouse and monkey MHC class I affinities for peptides of length 8-11. *Nucleic Acids Res* **36**, W509-512 (2008).
36. Nielsen, M*., et al.* Improved prediction of MHC class I and class II epitopes using a novel Gibbs sampling approach. *Bioinformatics* **20**, 1388-1397 (2004).
37. Linnemann, C*., et al.* High-throughput identification of antigen-specific TCRs by TCR gene capture. *Nat Med* **19**, 1534-1541 (2013).